Marine Analysis of WIG (Wing in Ground) and High Speed Catamaran

*Seung-Hyun Kwag**

〈 C o n t e n t s 〉

Abstract

Marine analysis was made to investigate the hydrodynamic effects of a Wing in Ground (WIG) by means of finite difference techniques. The air flow field around WIG is analyzed by the Marker & Cell (MAC) based method, and the interactions between WIG and the free surface are studied by showing pressure distributions above the free surface. In the latter part, computations are extended to make clear the flow characteristics of a high speed catamaran in the range of Froude numbers 0.2 to 1.0 with a separation to length ratios of 0.2, 0.3 and 0.5. The Navier-Stokes solver is invoked in which the nonlinear free-surface boundary condition is applied. For the validation, computational results are compared with the experiments.

I. Introduction

The wing in ground effect (WIG) demonstrates both features of the airplane and the ship. Because it gives us a newer concept of a highly efficient vessel operating over 100 knots. A wing operating in close proximity to the ground exhibits a reduction in induced drag, which increases the lift/drag ratio. In 1970s, the power augmented ram (PAR) phenomena were discovered, which significantly enhanced the performance of the WIG concept. Recently, an interest in the development of super-high speed ships are rapidly growing worldwide. Among several types of crafts along these lines, the PARWIG craft is a potential candidate for fast sea transport[1),(2)].

In the high speed catamaran, the free surface handling and wave-body interaction are related to the design of high speed vessels. Various hull forms such as hydrofoil crafts, planing boats, catamaran and surface effect ships have been developed to satisfy the design criteria, where catamaran Is one of the most practical hull

* Halla University, Wonju, Kangwondo, 220-712 Korea
Email: shkwag@hit.halla.ac.kr, Fax: 82-33-760-1138, Tel: 82-33-760-1233

forms due to the large deck area with small waterplane area, good transverse stability quality and unusual resistance property. Although a number of experimental and theoretical investigations such as Insel[3], Eggers[4], Turner [5], Everest[6], Fry[7] on the catamaran resistance have been conducted from the past, there is a lack in understanding on interference effects between the demihulls. In the present latter part, the effect of wave interference was investigated and the optimum hull spacing is sought by which the wave interference can be reduced, changing the s/L over a wide range of Froude numbers. The results between computation and experiment were quantitatively compared.

II. Numerical Scheme

2.1 Basic Equations and Boundary Conditions

The Navier-Stokes and continuity equations are governing ones. Pressures are obtained throughout the fluid domain by solving the Poisson equation. Iterations are stopped when the pressure difference between two consecutive approximations is smaller than a certain quantity, chosen as a priori. At the upstream boundary, the flow starts from zero and is accelerated up to the predefined speed. Thus, each horizontal component of velocity has the same constant value depending on the time step. The vertical component is equal to zero in each point of the upstream boundary and remains the same during the pressure computation. The pressure is the static one and remains the same, too. The bottom boundary is located far enough from the still water level. The pressure is set constant at the static value. On the body surface, the no-slip condition for the velocity and the Neumann condition for the pressure are used.

2.2 Free-Surface Boundary Condition

The fluid particle is moved by

$$\frac{\partial h}{\partial t} + u\frac{\partial h}{\partial x} - w = 0 \Big|_{z=z} \qquad (1)$$

The boundary condition for the free-surface requires zero tangential stress and a normal stress that balances any externally applied normal stress. The displacement of the particle is given by

$$\Delta x = u \cdot \Delta t \quad , \quad \Delta h = w \cdot \Delta t \qquad (2)$$

where Δt is the time increment. On the other hand, the use of an Euler-type expression of the kinematic free-surface boundary condition makes possible to employ a higher finite difference scheme. The condition can be written as follows:

$$\frac{\partial h_i^{n+1}}{\partial t} + (u_i + \frac{\partial u_i}{\partial z}\Delta h_i)\cdot\frac{\partial h_i^{n+1}}{\partial x} - w_i = 0 \qquad (3)$$

where $h = h(x, t)$ represents the elevation.
Expanding in Taylor series, the following can be obtained:

$$\frac{\partial h_i^{n+1}}{\partial t} = \frac{1}{2\Delta t}\cdot(h^{n-1} - 4h^n + 3h^{n+1}) \qquad (4)$$

For the $\partial h^{n+1}/\partial x$ derivative, the third order upwind difference(TOUD hereafter),

$$c\frac{\partial h}{\partial x} = c\frac{1}{6\Delta x}(-2h_{i-3} + 9h_{i-2} - 18h_{i-1} + 11h_i) \qquad (5)$$

where c is the convective velocity, can be decomposed into two parts. One is the central differencing term whose mathematical expression can be obtained by suitable Taylor expansions as follows:

$$\frac{c}{24\Delta x}(h_{i-3} - 27h_{i-2} + 27h_{i-1} - h_i) \qquad (6)$$

The other is the diffusion term, which has the meaning of the fourth derivative of the velocity.

$$\frac{3c}{8\Delta x}(-h_{i,-3}+7h_{i,-2}-11h_{i,-1}+5h_i) \tag{7}$$

The latter is expected to play a role to compensate the "finiteness" of the differentiation without phase shift. Here the third derivative contributes the phase shift without damping.

$$\frac{ac}{(\Delta x)^3}(-h_{i,-3}+3h_{i,-2}-3h_{i,-1}+h_i) \tag{8}$$

where $a=-\frac{(\Delta x)^2}{6}$ is a constant.

(8) is added to the right hand side term of (5), and the new formulation for the $\partial h/\partial x$ becomes,

$$c\frac{\partial h}{\partial x}=c\frac{1}{6\Delta x}(-h_{i,-3}+6h_{i,-2}-15h_{i,-1}+10h_i) \tag{9}$$

Introducing (4) and (9) into (3), the vertical coordinate increment at each time step can be,

$$\Delta h_i^n=\frac{3\Delta x(h_i^{n-1}-h_i^n)+\Delta t\cdot\{6u_i\Delta x+u_i(\Delta h_{i-3}^n-6\Delta h_{i-2}^n+15\Delta h_{i-1}^n-Q_i^n)\}}{9\Delta x+\Delta t\cdot[10u_i+Q_i^n\frac{\partial u_i}{\partial z}-6\Delta x\frac{\partial w_i}{\partial z}]} \tag{10}$$

The expression is of the second order accuracy for $h(O(h^2))$ for any $u>0$. Q_i^n, in (10) is

$$Q_i^n=-h_{i-3}^n+6h_{i-2}^n-15h_{i-1}^n+10h_i^n \tag{11}$$

where h at the $(n+1)^{th}$ step is calculated as

$$h^{n+1}=h^n+\Delta h^n \tag{12}$$

III. Computation and Discussions

3.1 WIG

Fig. 1 shows the coordinate system for the computation. Fig. 2 shows the sectional grid view. The number of grids are 101x32x44 for the air region and 101x32x10 for the water region. The Reynolds number is 10^3 for the laminar, and 10^6, 10, 10^8, 10^9 for the turbulent flow calculations.

Table 1 shows the comparison at 6° bewteen the present result and other investigators. Refer to Riegels[8] and Abbott[9]. The lift and drag coefficients are compared with those by Hirata[1] and BIEM, in which the lift shows a reasonable result in its trend.

Table 1 Comparison of lift and drag coefficients

	Present solver	Hirata	BIEM	Abbott
C_L	0.613	0.65	0.71	0.64
C_D	0.032	0.0117	-	0.0084

Table 2 Effect of PAR at h/c=0.10 and $\alpha=10°$

	C_L	Cf	C_p	C_D	C_L/C_D
off PAR	1.074	0.0106	0.081	0.092	11.7
PAR 1	1.291	0.0109	0.082	0.093	13.9
PAR 2	1.477	0.0113	0.082	0.093	15.9

Table 2 shows the PAR effect. When the body approaches the ground, the velocity becomes smaller below the wing surface due to the PAR effect and the lift becomes larger due to the pressure increase. The thrust is applied in the form of uniform flow for the PAR 1 and -45° inclined flow for the PAR 2. The PAR is located in front of the leading edge, off half the chord length. To investigate the effect of PAR, the propulsor is artificially placed in the upstream of wing and the flow is accelerated through the wing with a 10° angle of attack for the analysis. The thrust gives 30% increase in the velocity by the momentum theory. Fig. 3 shows the results

of non free-surface case. Table 3 shows the effect of angle of attack. Fig. 4 shows the results of the non free-surface case at height/chord of 0.3, Froude number of 6.87, with a 10° angle of attack. Since the flow speed is very fast in this case, the pressure gradient generated by the

Table 3 Effect of angle-of-attack(α) at h/c=0.8

	C_L	Cf	Cp	C_D
α=10°	0.7295	0.0101	0.074	0.084
α-6°	0.6136	0.0099	0.032	0.042
α-4°	0.5616	0.0104	0.028	0.038

leading edge is strongly affected by the free surface. The free surface renders the pressure gradient much steeper, especially around the tip.

Fig. 5 shows the results at Reynolds number of 10^6 with the angles of attack 6° and 10° in which the height/chord is 0.1 from free surface. The pressure is well developed even at the high Reynolds number flows. For the high Reynolds number flow simulations, the Baldwin Lomax turbulence model is used.

Fig. 6 shows the results at the Reynolds number of 10^6, 10^8, 10^{10} from above in which the Froude number is 3.5, with a 3.5° angle of attack. Even at very high speeds, these reliable results are obtained. This supports that the MAC based code is very useful for the free surface computations.

3.2 Catamaran

As the first example, the catamaran with Wigley demihulls was tested at Froude number of 0.289, 0.316, 0.5, 0.6 1.0 and s/L of 0.2, 0.3 0.5. Fig. 7 shows the grid view for the catamaran. The grid is made as H-H topology to treat the free surface movement more conveniently. The wave height contours are shown in Fig. 8 and Fig. 9 in which the Froude number and s/L are changed. As the s/L becomes smaller, the divergent wave between the demihulls is eliminated and the transverse wave is dominant due to the divergent wave interference. In case of s/L=0.5, the wave interference almost disappears and the wave pattern becomes similar to that of monohull. The effect of wave interference between the demihulls is dominant as the s/L becomes smaller and in the case of s/L=0.2, as the wave interference become larger, the effect is propagated to outer flow fields at the outer side of the demihulls. The results of computation are qualitatively well agreed with experiments. The wave resistance interference factors τ, for different s/L, are given in Fig. 10, which is defined as C_w(catamaran)/C_w(monohull). Although the test points are not enough, the wave interference can be effectively neglected above the particular speed which is separation dependent and indicates that higher separation results in a smaller interference.

The second example of catamaran is the displacement type moving at two Froude numbers of 0.45, 0.95. Fig. 11 shows the wave heights in which the results of monohull are compared in (a) and (b), while those of twin-hull are in (c). By the wave height, the effects of Froude number can be clearly seen. Fig. 12 shows the velocity vectors inside the hulls. Fig. 13 shows the photos for the stern waves at two speeds, which was taken at the towing tank of Hyundai Heavy Industry.

IV. Conclusion

(1) The marine analysis of WIG was made by the

MAC-based method, and the interactions between WIG and the free surface are investigated. The results show that the effect of the free surface is negligible in the generation of waves, when compared to the results in which the free surface is assumed to be a rigid wavy wall. But the pressure patterns are slightly different between the non free-surface case and free-surface case when the body approaches the free surface.

(2) The marine characteristics for a high speed catamaran was investigated by comparing the calculated wave resistance with the experiments. The effect of wave interference is reviewed, and the optimum hull spacing is sought by which the wave interference can be reduced, changing the s/L over a wide range of Froude numbers.

References

(1) Hirata, N., "Simulation on Viscous Flow around Two Dimensional Power Augmented Ram Wing in Ground Effect", SNAJ, Vol. 174, pp. 47-54, 1993

(2) Hirata, N., "Numerical Study on the Aerodynamic Characteristics of a 3-D Power Augmented Ram Wing in Ground Effect", SNAJ, Vol. 179, pp. 31-39, 1996

(3) Insel, H. and Molland, A. F., "An Investigation into the Resistance of High Speed Displacement Catamarans", Trans, RINA, 1991

(4) Eggers, K., "Resistance Conditions of Two Body Ships", Jahrbuch der Schiffbautech Gesellshaft, Vol. 49, 1995

(5) Turner, H. and Taplin, A., "The Resistance of Large Powered Catamarans", Trans. SNAME, Vol. 76, 1968

(6) Everest, J. T., "Some Research on the Hydrodynamics of Catamarans and Multi Hulled Vessels in Calm Water", Trans. NECIES, Vol. 84, 1967

(7) Fry, E. D. and Graul, T., "Design and Application of Modern High-Speed Catamarans", Marine Technology, Vol. 9, No. 3, 1972

(8) Riegels, F. W., "Aerofoil Sections", Butter Worths, London, 1961

(9) Abbott, I. H. and Von Doenhoff, A. E., " Theory of Wing Sections", Dover Publication, New York, 1958

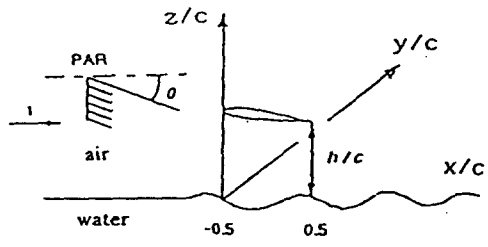

Fig. 1 Definition of coordinate system

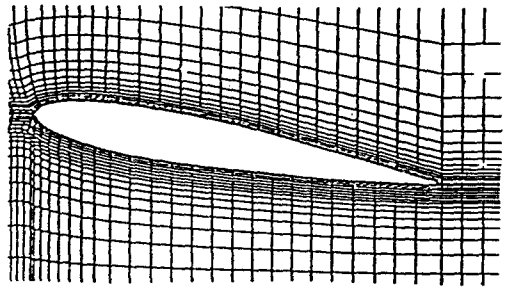

Fig. 2 Sectional view of grid generation

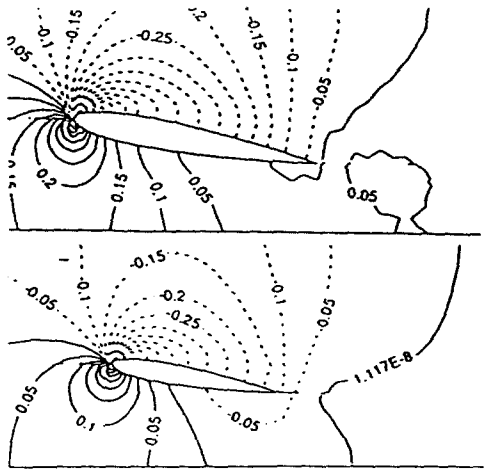

Fig. 3 Pressure contours without free surface at Froude number of 2.29

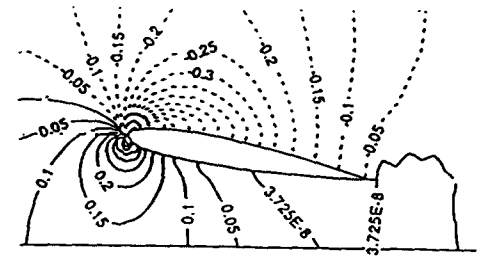

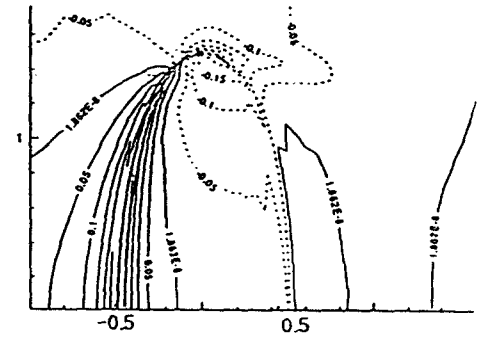

Fig. 4 Pressure contours without free surface at Froude number of 6.87

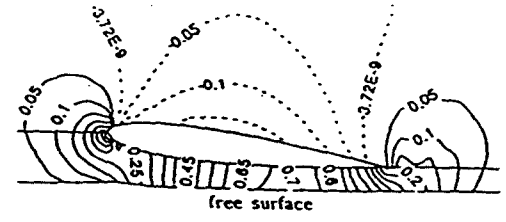

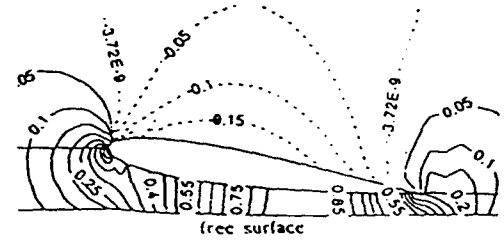

Fig. 5 Pressure contours with free surface at Fn=3.5, Rn=10^6, α=6, 8° from above

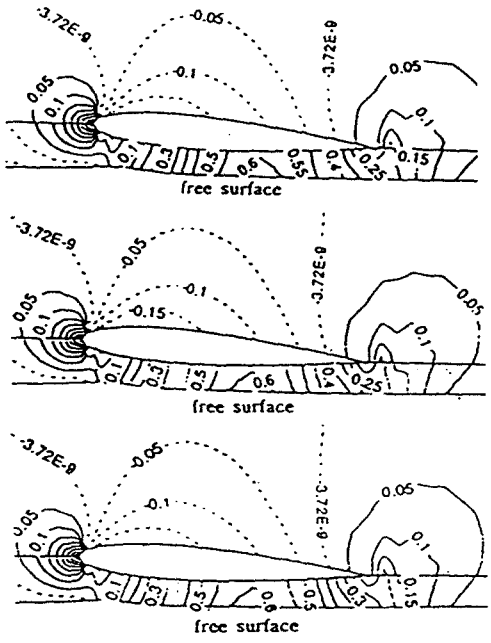

Fig. 6 Pressure with free surface at Fn=3.5, α=3.5° , Rn=10^6,10^8,10^{10} from above

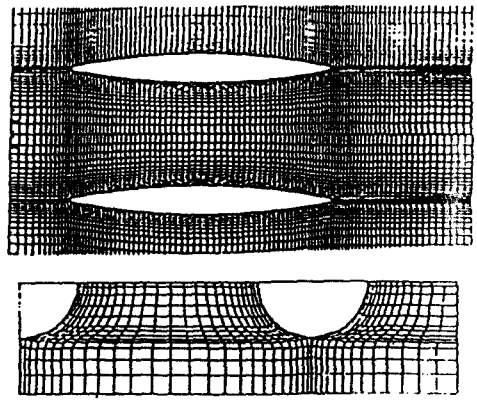

Fig. 7 Grid generation of catamaran

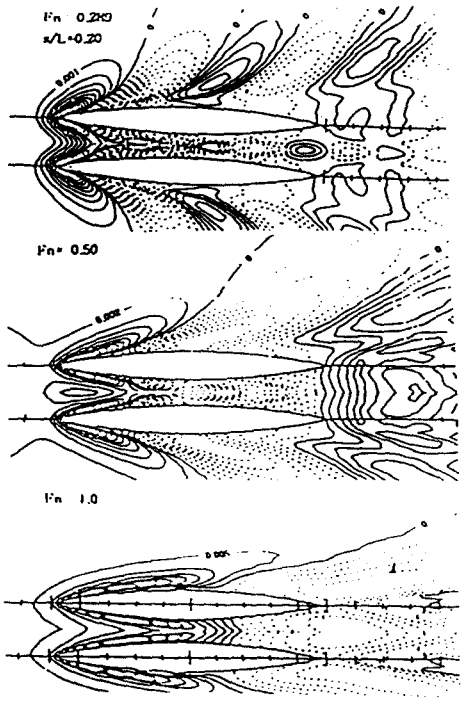

Fig. 8 Wave height contours at s/L=0.20 at Fn=0.289, 0.50, 1.0 from above

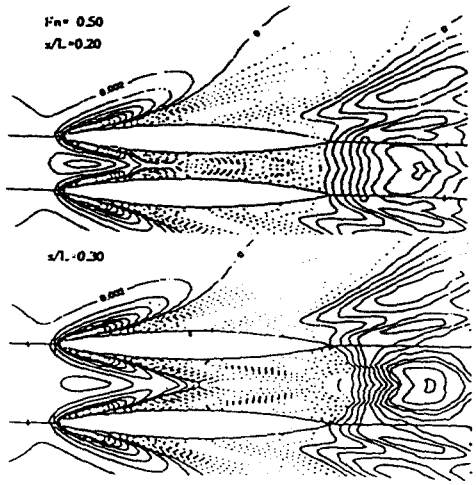

Fig. 9 Wave height contours at Fn=0.50 at Fn=0.20, 0.30, 0.50 from above

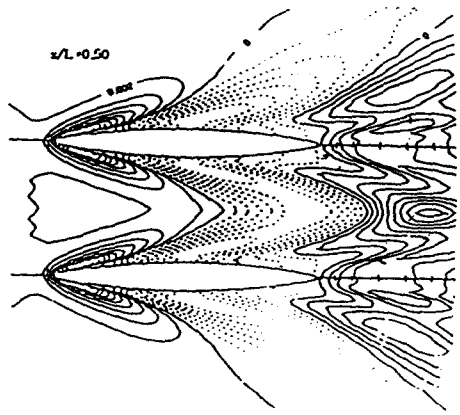

Fig. 9 (continued)

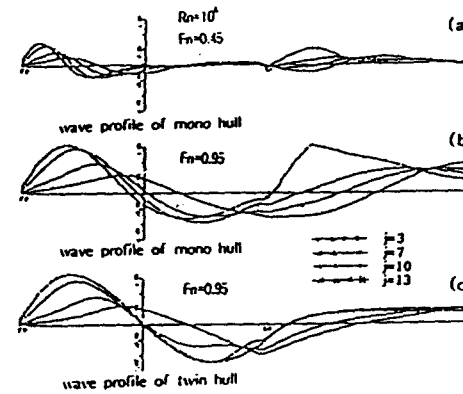

Fig. 11 Wave height for mono and twin hull

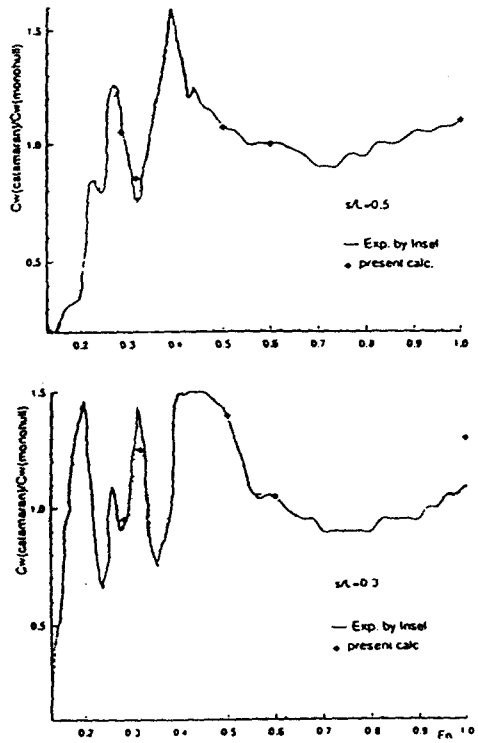

Fig. 10 Wave resistance interference factor τ

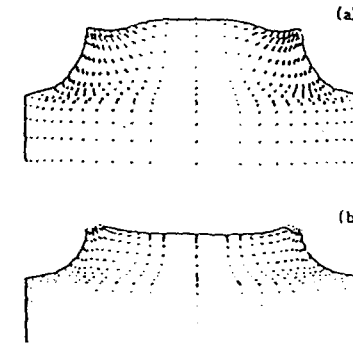

Fig. 12 Velocity vectors for catamaran
(a) x/L=0.55 (b) x/L=0.90

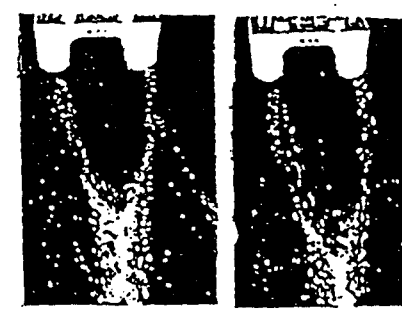

Fig. 13 Photos for stern waves of catamaran
4.5m/sec, 5.0 m/sec from l.h.s.